LEGIBILITY NOTICE

A major purpose of the Technical Information Center is to provide the broadest dissemination possible of information contained in DOE's Research and Development Reports to business, industry, the academic community, and federal, state and local governments.

Although a small portion of this report is not reproducible, it is being made available to expedite the availability of information on the research discussed herein.

LA-UR--88-4290

DE89 005470

TITLE: MODELING of LASER ABLATION and FRAGMENTATION of HUMAN CALCULI

AUTHOR(S): Steven Gi[redacted]er, X-1
Roger D. Jones X-1
Charles Howsare Uniform Services University

SUBMITTED TO: SPIE Symposium on Medical Applications of Lasers & Optics
15-20 January 1989, Los Angeles, CA

DISCLAIMER

Los Alamos National Laboratory
Los Alamos, New Mexico 87545

FORM NO. 836 R4
ST. NO. 2629 5/81

MODELING OF LASER ABLATION AND FRAGMENTATION OF HUMAN CALCULI

S.J. Gitomer & R.D. Jones, Los Alamos National Laboratory, Los Alamos, NM 87545 and
C. Howsare, Uniform Services University, Bethesda, Maryland 20814-4799

ABSTRACT

The large-scale radiation-hydrodynamics computer code LASNEX, has been used to model experimental results in the laser ablation and fragmentation of renal and biliary calculi. Recent experiments have demonstrated laser ablation and fragmentation of human calculi *in vitro* and *in vivo*. In the interaction, laser light incident upon the calculus is of sufficient intensity to produce a plasma (a hot ionized gas). The physical picture which emerges is as follows. The plasma couples to acoustic and shear waves which then propagate through the dense stone material, causing spall and fracture by reflection from material discontinuities or boundaries. Experiments have thus far yielded data on the interaction against which models can be tested. Data on the following have been published: (1) light emission, (2) absorption and emission spectra, (3) fragmentation efficiency, (4) cavitation bubble dynamics and (5) mass removal. We have performed one dimensional simulations of the laser-matter interaction to elucidate the important physical mechanisms. We find that good quantitative fits between simulation and experiment are obtained for visible light emission, electron temperature, electron density, plasma pressure and cavitation bubble growth. With regard to mass removal, experiment and simulation are consistent with each other and give an excellent estimate of the ablation threshold. The modeling indicates that a very small ablation layer at the surface of the calulus is responsible for significant mass loss by fragmentation within the bulk of the calculus. With such quantitative fits in hand, we believe this type of modeling can now be applied to the study of other procedures involving plasma formation of interest to the medical community.

INTRODUCTION

Over the past ten years, there has been considerable progress in the non-surgical destruction and removal of human calculi. Ultrasound lithotripsy, the first of the modern nonsurgical removal methods, today enjoys widespread application. Another method, laser mediated lithotripsy, was first reported in 1985 [1]. In this technique, laser pulses from a high power dye laser (typical wavelength 500 - 700 nm, pulselength 1 μsec, intensity 10^8 W/cm^2, pulse repitition rate 5 Hz) are delivered to the calculus via a fiber optic cable passed into the body through a ureteroscope. Tens to hundreds of laser pulses were needed to vaporize/fragment stones of most material compositions. Success rates in clinical studies in excess of 90% have been reported [2]. *In vitro* experiments have shown that, in order for vaporization/fragmentation of the stones to occur, a gaseous plasma (ionized gas) must be present.

Modeling of laser-matter interactions, in which a plasma is present, has been the province of laser-fusion researchers for many years [3]. Tools developed within this community, for high intensity, short pulse lasers, may be applied with small modification to the physical interaction we are considering here. The tools to which we refer are large scale radiation-hydrodynamic computer models which propagate laser light, use equations of state and tabular opacities for specific materials of interest, follow plasma evolution in one or two spatial degrees of freedom, etc [4]. Such models are to be contrasted with simpler mathematical models [5], intended to apply to laser matter interactions in which heating of the target materials occur - *but not plasma formation*. Models [5] approach the desired intensity range of 10^8 W/cm^2 from below while other researchers [6] have explored intensities which approach our target intensity from above. We believe that we are the first to explore the given laser intensity region with a large scale computer code applied to the study of the calculi.

This paper is organized into sections as follows. First, we summarize the experimental data available to date and the proposed mechanism for the laser-calculus interaction. Next, we briefly describe our model and present results obtained therefrom. Finally, we summarize this work and draw conclusions.

EXPERIMENTAL RESULTS AND PROPOSED MECHANISM

In a series of *in vitro* experiments, a number of important effects have been observed for lasers interacting with calculi. Pulsed dye lasers were shown to be able to fragment calculi rather efficiently. As much as 2% of calculus

GITOMER

mass could be removed per pulse at the highest laser energies used [7]. The fragmentation of calculi relies upon the threshold for plasma production to be exceeded [8]. A signature of the plasma production is optical emission during and after the laser pulse. The optical signal is characterized by broadband continuum emission at early times (a few hundred ns after the beginning of the laser pulse) followed by the development of strong emission lines (identified with excited and singly ionized Ca) at later times (a μs or more after the beginning of the laser pulse). Blackbody spectral fits to the optical continuum emission yield temperature values of the order of a few thousand ^{o}K. Electron densities of the order of 10^{19} electrons/cm^3 have been inferred from the spectral line widths [8]. Experiments have shown the presence of strong acoustic waves propagating through target stones [9]. Coupling of the laser to the stones, as measured by the strength of the acoustic waves, was substantially enhanced when the stones were immersed in water compared to the case for stones in air [10]. Also observed were cavitation bubbles, for the immersed stone experiments, with bubble lifetimes of the order of 1 ms (laser pulses were always about 1 μs in duration) [9]. Pressure transients in the region between the calculus surface and the end of the fiber optic delivery cable were estimated to be in the 1 KBar range [9].

The mechanism proposed [10] to explain the laser-calculus interaction proceeds as follows. The laser interacts with the opaque stone surface producing a thin localized heated layer. As the heating continues, there is vaporization, liberation of free electrons and plasma formation. Alternatively, there can be material desorption from the stone surface followed by heating and free electron creation in the desorbed material [11]. The plasma continues to absorb the laser light, likely by inverse bremsstrahlung absorption. Then the plasma expands either freely (in air) or mechanically constrained (in water) and creates a back pressure on the stone surface. Evidence of this back pressure has been seen experimentally in the rapid recoil of the fiber optic delivery cable on time scales of the order of a few microseconds [9]. The pressure induces strong acoustic waves (stress waves) within the stone material [9]. These waves are compressive stress waves initially. Upon reflection from internal stone inhomogeneities or from the stone-air or stone-water interface, the waves become tensile stress waves of sufficient strength to fragment the stone [12].

SIMULATION MODEL

In this work, we use the LASNEX radiation-hydrodynamics computer code to simulate the behavior of the laser-calculus interaction. The details of the physical model which LASNEX uses are presented in Ref. 4. Briefly stated, the code treats an initial plasma of ions and electrons absorbing laser light of a given wavelength and emitting and/or absorbing a spectrum of radiation at wavelengths near that of the source laser. Hydrodynamic equations are solved for the evolution in time of one fluid with temperatures for electrons and ions, yielding positions, velocities, temperatures, densities and pressures. A multigroup (that is, many wavelength groups) radiation treatment is employed to treat the emission and absorption of the spectrum of radiation appropriate to the laser-calculus interaction. Real materials are treated using tabular equations-of-state (which give material pressure for specified material density and temperature) [13]. Radiation characteristics are obtained using tabular wavelength dependent emission and absorption opacities computed for the specific materials of interest [14]. Figure 1 shows in schematic form how the simulation proceeds.

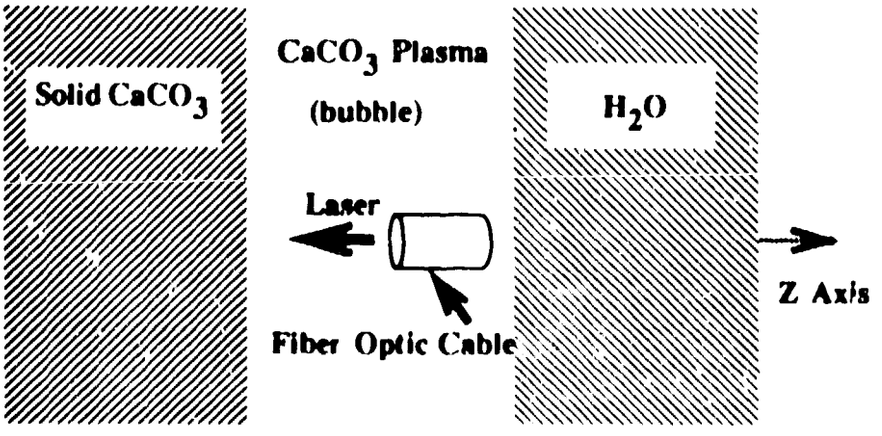

Figure 1. Schematic of 1D LASNEX simulation. Laser pulse reaches opaque stone material via a fiber optic delivery cable. Laser pulse temporal evolution matches experiment. As simulation proceeds, a bubble forms between the solid stone and the water. Only motion in the z direction is permitted.

Laser light is absorbed using the inverse bremsstrahlung absorption mechanism [15]. This mechanism depends upon the existence of a plasma. Consequently, we do not model well the initial absorption of energy and the plasma formation phase of the interaction. In order

to model laser absorption at material temperatures below 10,000 ^{o}K and at laser intensities of about 10^8 W/cm^2, however, the percentage of ionization, which is used in the formula for inverse bremsstrahlung, is adjusted. We use values in the code, consistent with Saha equilibrium results, to yield initial absorption depths in the simulation which approximate those found experimentally for cold stone material [16]. We model calculi here using the equation-of-state for $CaCO_3$ (taken as a representative calculus material) with an initial cold mass density of 1.2 gm/cm^3 (measured from sample calculi). We note here that the physics of fragmentation is not treated by LASNEX and thus would need to be studied using a solid material code. We report here only on calculations performed with one spatial degree of freedom.

SIMULATION RESULTS

Preliminary results of this research have been previously reported [17]. We present here a quantitative comparision between our simulation results and those obtained from experiments cited above. First, consider visible light emission. Broadband visible light emission is one of the signatures of pulsed-laser calculus interaction. Such emission always accompanies calculus fragmentation. Time resolved broadband (400 to 700 nm band) signals have been measured [8]. Figure 2 shows the experimental laser pulse and the broadband emission signal, plotted with peak intensities normalized to unity for ease of comparison. One notes that the emission signal begins later than, rises as rapidly as, peaks later than, and falls more slowly than the driving laser pulse. The radiation spectrum which is computed by LASNEX may be processed to yield a comparable broadband emission signal. The result is shown as the dotted curve in the figure. Although both simulation and experimental emission signals have the same general shape and time of onset, the simulation signal shows a slower initial growth and later peak than the experiment. This disagreement is due to poor modeling of the initial plasma formation.

Optical spectra obtained in the experiments show prominent line emission [8]. Identification of some of the lines with excited and singly ionized Ca has been made. One can thus take the first ionization potential of Ca (6.1

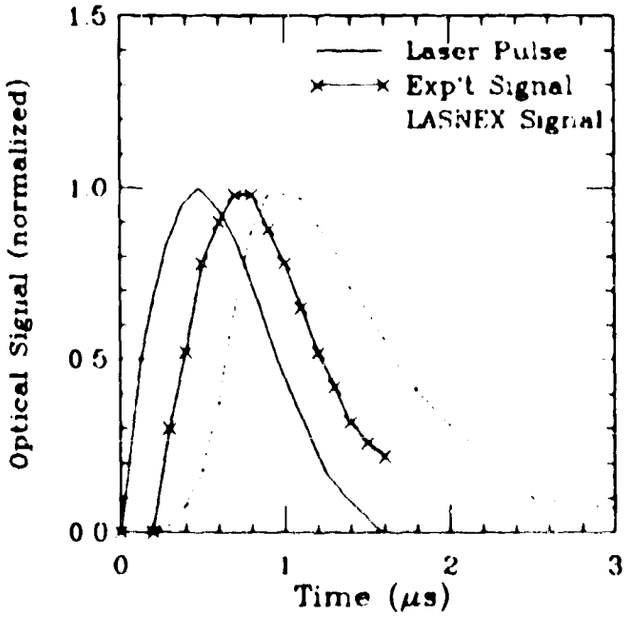

Figure 2. Optical signal (normalized) plotted versus time (μs). Laser pulse (solid curve) is at a 690 nm wavelength. Experimental broadband emission signal (X's) covers the 400 nm to 700 nm band. LASNEX broadband emission signal spans the 400 nm to 700 nm band.

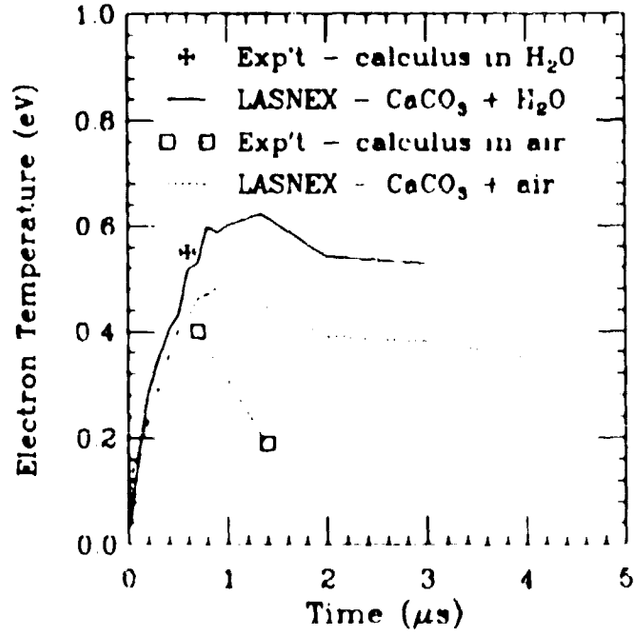

Figure 3. Electron temperature (eV) versus time (μs). Experimental results for calculi in H_2O and in air are indicated by a cross or squares, respectively. LASNEX results for $CaCO_3$ in H_2O and in air are indicated by solid or dotted curves, respectively.

eV) to give an order of magnitude estimate of the plasma electron temperature to be expected in the laser produced plasmas present here (recall that 1 eV = 11600 ^{o}K). Experiments with lasers interacting with metals have yielded electron temperatures of 1.4 to 4.0 eV for lasers with intensities of 10^8 W/cm^2 [18]. Such values are expected to overestimate temperatures for calculi in which absorption in depth, rather than the surface absorption of metals, is anticipated. Finally, one can fit a blackbody spectrum to the published spectral data for calculi [8] and obtain a temperature of approximately 0.6 eV. In Fig. 3, we show plots of the LASNEX results for electron temperature versus time for (1) $CaCO_3$ in air and (2) $CaCO_3$ in water. Displayed as well are approximate electron temperature values obtained experimentally (from ratios of spectral line intensities) [19]. There is agreement between simulation and experiment on the magnitude of the electron temperature. The temperature appears to fall more slowly with time for the simulations than for the experiments.

The emission spectra can be used, as well, to estimate electron density. In this case, standard formulas relating line width to electron density are used [20]. An experimental determination was made of electron density [8] yielding 10^{19} electrons/cm^3 over a time interval from 0.64 to 0.90 μs after the start of the laser pulse. In Fig. 4, this result is plotted along with simulation results of electron density as a function of time for both $CaCO_3$ in water and $CaCO_3$ in air. The experimental points agree with LASNEX simulations in air.

Experimental studies of acoustic/stress wave propagation through calculi have been reported [9]. These studies show that there is a tenfold enhancement of optoacoustic and piezoelectric signals when calculi are immersed in water as compared to calculi in air. Our simulation model, dealing as it does with plasma, cannot provide direct information on acoustic/stress waves in solids. Nevertheless, we believe that it is the plasma pressure, generated by the laser pulse at the stone surface, which drives the acoustic/stress wave into the stone. LASNEX computes plasma pressures given local material density and temperature (from the equation-of-state tables). Results of our calculations are shown in Fig. 5. Here, plasma pressure is plotted as a function of time. Note that the plasma pressure for $CaCO_3$ in H_2O is on the average 4 to 5 times greater than the result for $CaCO_3$ in air. This result is in substantial

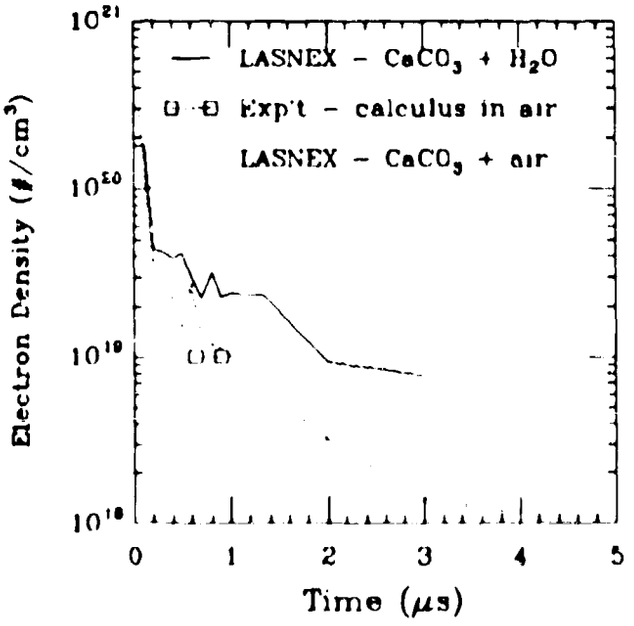

Figure 4. Electron density (electrons/cm^3) versus time (μs). Experimental results for calculus in air are indicated by squares. LASNEX results for $CaCO_3$ in H_2O and in air are indicated by solid or dotted curves, respectively.

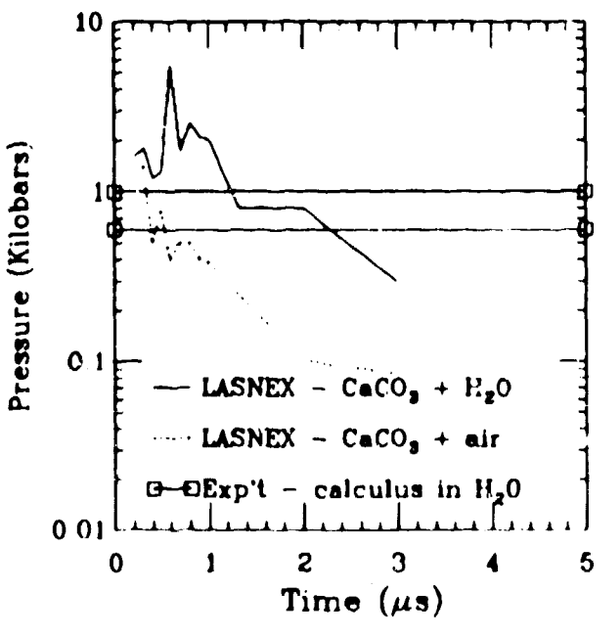

Figure 5. Plasma pressure (kilobars) versus time (μs). Experimental estimates for calculus in water is indicated by the horizontal lines ended with squares. LASNEX results for $CaCO_3$ in H_2O and in air are indicated by solid or dotted curves, respectively.

agreement with those reported in Ref. 9.

It is worth noting that quantitative estimates of the plasma pressure have also been made [9]. The values obtained are 0.6 Kbar (using data on cavitation bubble evolution in water) and 1.0 Kbar (using measured recoil of the fiber optic delivery cable). These are consistent with experimental values obtained by others [21]. The estimates for calculi in water are also in excellent agreement with the LASNEX results shown in Fig. 5.

Experiments on calculi immersed in water have shown the presence of cavitation bubbles [9]. These bubbles grow in time to a diameter of nearly 1 cm over a time span of about 250 μs. After reaching a maximum diameter, the bubbles decay. Time resolved measurements of cavitation bubble evolution have been made using both a pump-probe laser technique and microsecond duration flash photography. The LASNEX simulations, likewise, show the presence of such cavitation bubbles. These appear as mass density depressions in the $CaCO_3$, growing in size over time. In Fig. 6, we plot in a log-log display the experimental and LASNEX simulation results for bubble diameter as a function of time. There is good agreement between the two in their region of overlap. For long times, the experimental results may be compared (at least as to slope) with analytic results on bubble diameter growth [22]. The predicted time dependence of $t^{2/5}$ is plotted as a dotted curve in the Figure overlaying the experimental results. Here too, excellent agreement is seen.

Finally, consider the experimental results on mass removal [23]. Data is presented for the total mass of fragments removed from sample stones by a single laser pulse of a given energy. Fragment sizes ranged from less than 150 μm to greater than 2 mm in diameter, the distribution of mass into a number of fragment size ranges being very dependent on laser energy. Mass lost per laser pulse (μg) is plotted versus laser energy (mJ) in Fig. 7, where the experimental results for a 504 nm pulsed dye laser are denoted by X's. Lost mass in the simulation is the portion of the $CaCO_3$ whose mass density has decreased to less than 50% of the initial density (1.2 gm/cm^3). LASNEX results are denoted by the squares. The simulation and experiment are consistent with each other for the following reasons. As stated above, LASNEX is a plasma simulation code, predicting as it does the behavior of an ionized gas.

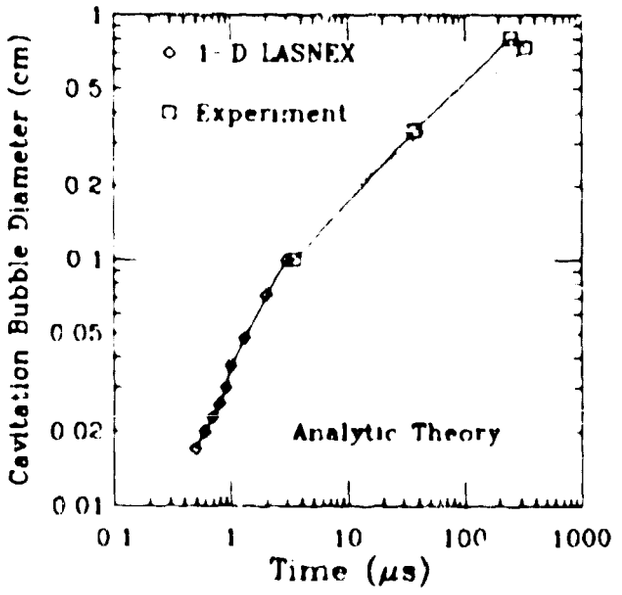

Figure 6. Cavitation bubble diameter (cm) versus time (μs). Experimental points are denoted by squares and connected with a solid line. LASNEX results are denoted by diamonds and are connected with a solid line. Analytic theory results is plotted as a dotted line.

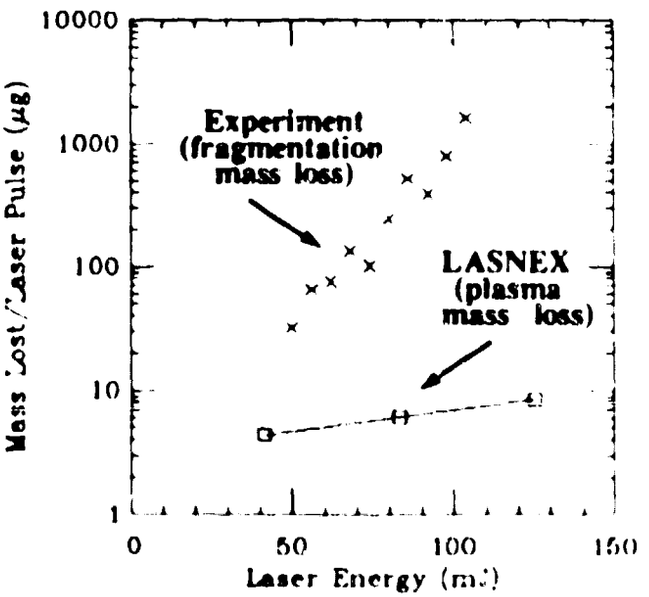

Figure 7. Mass lost per laser pulse (in μg) plotted versus laser energy (in mJ). Experimental points derived from Ref. 23 are denoted by X's. LASNEX simulation points are denoted by squares.

The experiments always produced *plasmas and fragments of stone*. Thus the experimental values will always equal or exceed the LASNEX predictions of *mass lost as plasma alone*. We would expect the code and experiment to yield the same result near the threshold for plasma production. One estimates such a threshold from the Figure to be at a laser energy of about 20 mJ, where extrapolations of simulation and experimental results cross. Experimental studies of ablation threshold (minimum laser energy need to produce visible damage on a stone's surface) yield threshold laser energies from 5.6 to 20.6 mJ depending upon laser wavelength [24] - in good agreement with our estimate. As can be seen from the Figure, at energies greater than 20 mJ, only a small fraction of the total lost mass is in the form of plasma. Most of the mass loss is in the form of fragments. The figure demonstrates how efficient the process is of mass removal in the laser calculus interaction.

CONCLUSIONS

We have modeled the interaction of pulsed lasers with human calculi, using a large-scale radiation hydrodynamics code LASNEX. We have modeled a body of experimental data to help elucidate the physical phenomena taking place here. Experimental data on light emission, absorption and emission spectra, fragmentation efficiency, cavitation bubble dynamics and mass loss, were considered. We have obtained good agreement between experiment and simulation with LASNEX on visible light emission, electron temperatures, electron densities, plasma pressures and cavitation bubble dynamics. Regarding mass loss, experiment and simulation were consistent with each other. In the experiment, mass was removed from the stones in the form of plasma and material fragments. In the simulation, only mass in the plasma state was removed. An extrapolation of mass loss results to low laser energies yielded an estimate of ablation threshold, in good agreement with experiment.

It is worthwhile to note that data on line spectra and on fragmentation have not been modeled. Further studies with LASNEX, with possibly a more realistic laser absorption model, are required to treat the line spectra. With regard to fragmentation, the subject needs to be investigated using yet another simulation code (e.g CHART-D [25]), one which treats solids. Such a code would require as an input energy source, the time dependent laser generated pressure computed by LASNEX.

We believe that the type of modeling study presented here can be fruitfully applied to other procedures of interest within the medical community - procedures in which a laser-produced plasma is present.

ACKNOWLEDGEMENTS

The authors wish to acknowledge useful discussions concerning this research with our colleagues at Los Alamos R. Dingus, S.R. Goldman, R.A. Kopp, members of the LASNEX Team, T. Loree, B.S Birmingham, and with our fellow scientists at other institutions P. Herring, P. Teng, T. Deutsch, R. Waynant, ..J. Welch and R. Straight. This work was performed under the auspices of the United States Department of Energy.

REFERENCES

1. G.M. Watson, S.L Jacques, S.P. Dretler, and J.A. Parrish, "Tunable Pulsed Dye Laser for Fragmentation of Urinary Calculi," Lasers Surg. Med. 5, 160 (1985) (Abstract).
2. S.P. Dretler, G.M. Watson, S. Murray and J.A. Parrish, "Laser Fragmentation of Ureteral Calculi: Clinical Experience," Lasers Surg. Med. 6, 191 (1986) (Abstract).
3. See for example S.J. Gitomer, R.D. Jones, F. Begay, A.W. Ehler, J.F. Kephart, and R. Kristal, "Fast Ions and Hot Electrons in the Laser-Plasma Interaction," Phys. Fluids 29, 2679 (1986) and references therein.
4. G.B. Zimmerman and W.L. Kruer, Comments Plasma Physics Controlled Fusion 2, 85 (1975).
5. A.J. Welch, "The Thermal Response of Laser Irradiated Tissue" IEEE J. Quant. Electron. QE-20, 1471 (1984)
6. S.R. Goldman, G.H. Canavan, R.S. Dingus, and M.A. Mahaffy, "Simulation of the Interaction of Single-Pulsed Optical Lasers with Targets in a Vacuum," in Gas Flow and Chemical Lasers, 1984, A.S. Kaye and A.C. Walker, eds., (A. Hilger, Ltd, London, 1985), and S.R. Goldman, S.J. Gitomer, R.A. Kopp, J. Saltzman, and R.S. Dingus, "Simulation of Laser Target Interaction in Vacuum," AIAA Conf. on Laser Effects and Target Response, Stanford Res. Inst., Menlo Park, CA, 5-7 Nov. 1985 (also Los Alamos National Laboratory Report LA-UR-85-4047, 1985).

7. R. Rox Anderson, N. Nishioka, S. Dretler and J. Parrish, "Pulsed Laser Fracturing of Renal & Biliary Stones," Conference on Lasers and Electro-Optics, 9-13 June 1986, San Francisco, CA, paper TUP1, pps 136-137 in Digest of Technical Papers (Abstract).
8. P. Teng, N.S. Nishioka, R.R. Anderson, and T.F. Deutsch, "Optical Studie of Pulsed-Laser Fragmentation of Biliary Calculi," Appl. Phys. B 42, 73 (1987).
9. P. Teng, N.S. Nishioka, R.R. Anderson, and T.F. Deutsch, "Acoustic Studies of the Role of Immersion in Plasma-Mediated Laser Ablation," IEEE J. Quant. Electron. QE-23, 1845 (1987).
10. N.S. Nishioka, P. Teng, T.F. Deutsch, and R.R. Anderson, "Mechanism of Laser-Induced Fragmentation of Urinary and Biliary Calculi," Lasers in the Life Sciences 1, 231 (1987).
11. S.E. Egorov, V.S. Letokhov, and A.N. Shibanov, "Mechanism for Ion Formation by Irradiation of Molecular Crystal Surfaces with Laser Pulses," Sov. J. Quantum Electron. 14, 940 (1984).
12. H. Kolsky, Stress Waves in Solids, (Dover, New York, 1963).
13. B.I. Bennett, J.D. Johnson, G.I. Kerley, and G.T. Rood, "Recent Developments in the Sesame Equation-of-State Library," Los Alamos Scienctific Laboratory Report LA-7130 (February 1978).
14. W.F. Huebner, A.L. Merts, N.H. Magee, and M.F. Argo, "Astrophysical Opacity Library," Los Alamos Scienctific Laboratory Report LA-6760-M (August 1977).
15. L. Spitzer, Jr., Physics of Fully Ionized Gases, (Interscience, New York, 1962), p. 148.
16. F.H. Long, N.S. Nishioka, and T.F. Deutsch, "Measurement of the Optical and Thermal Properties of Biliary Calculi Using Pulsed Photothermal Radiometry," Lasers Surg. Med. 7, 461 (1987).
17. S.J. Gitomer & R.D. Jones, "Modeling Laser Ablation and Fragmetation of Renal & Biliary Stones," Conference on Lasers and Electo-optics, Baltimore MD 26 April - 1 May 1987, Digest of Technical Papers, paper TUP5, p. 102 (Abstract) and 1987 IEEE International Conference on Plasma Science, paper 6C11, IEEE Conf Record 87CH2451-3, page 117 (1987) (Abstract) and S.J. Gitomer & R.D. Jones, "2-D Modeling Laser Ablation & Fragmentation of Biological Calculi," 1988 IEEE International Conference on Plasma Science, paper 6C1, IEEE Conf Record 88CH2559-3, page 136 (1988) (Abstract).
18. J.F. Ready, Effects of High-Power Laser Radiation, (Academic, New York, 1971), p. 192 - 193.
19. Preliminary results with possibly large error bars were provided to us by P. Teng, N.S. Nishioka, R.R. Anderson, and T.F. Deutsch, private communication (1987).
20. H.R. Griem, Spectral Line Broadening by Plasmas, (Academic, New York, 1974).
21. N.C. Anderholm, "Laser-generated Stress Waves," Appl. Phys. Lett. 16,113 (1970); H.D. Fair, "In Vitro Destruction of Urinary Calculi by Laser-induced Stress Waves," Med. Instrum. 12, 100 (1978).
22. R.H. Cole, Underwater Explosions, (Princeton University Press, Princeton NJ, 1948).
23. G.M Watson, S.P. Dretler and J.A. Parrish, "The Pulsed Dye Laser for Fragmentation of Urinary Calculi," preprint (1986).
24. N.S. Nishioka, Paul C. Levins, S.C. Murray, J.A. Parrish, and R.R. Anderson, "Fragmentation of Biliary Calculi with Tunable Dye Lasers," Gastroenterology 93, 250 (1987).
25. S.L. Thompson, "CHART D: A Computer Program for Calculating Problems of Coupled Hydrodynamic Motion and Radiation Flow in One Dimension," Sandia Laboratories, Albuquerque, NM, Report SC-RR-69-613, November 1969.